JPRS-UMS-90-003
1 MAY 1990

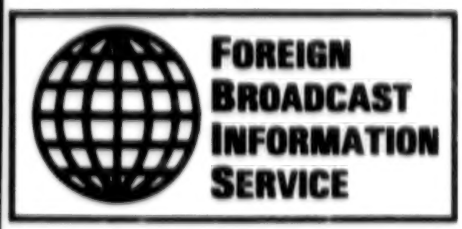

JPRS Report

Science & Technology

USSR: Materials Science

JPRS-UMS-90-003
1 MAY 1990

SCIENCE & TECHNOLOGY

USSR: MATERIALS SCIENCE

CONTENTS

PREPARATIONS

MISCELLANEOUS

UDC 621.78:535.211

Laser Alloying of Steel Using Powder Materials

907D0092A Minsk IZVESTIYA AKADEMII NAUK BELORUSSKOY SSR: SERIYA FIZIKO-TEKHNICHESKIKH NAUK in Russian No 4, Oct-Dec 89 (manuscript received 20 Oct 80) pp 7-13

[Article by S. A. Astapchik, V. S. Golubev, O.V. Novikova, L. I. Protskevich, and I. S. Chebotko, Engineering Physics Institute at the Belorussian Academy of Sciences]

[Text] Operating properties of metals and alloys can be improved by laser alloying; in essence, this process amounts to melting a surface segment together with the alloying elements added to it, thus making it possible to obtain a new alloy with given properties within a local volume. Compared to known methods of chemical processing and heat treatment, the laser alloying method has a number of advantages: alloying materials are saved, there is no need for subsequent heat treatment; the volume of subsequent machining is minimal; the process rate and product quality are high, etc. To date, a number of studies have been completed [1–3] in which the laser alloying process was performed using various installations and was conducted under various conditions. Consequently, we are facing the important task of classifying the resulting data which, in the final analysis, will make it possible to optimize the alloying process.

In this article, we examine the possibility of laser alloying of the surface of steels 45, 5KhNM, and Kh12F1 in order to increase their heat stability and wear resistance. Both annealed samples and samples subjected to a standard hardening heat treatment beforehand were used in this research. Samples covered by an alcohol-based coating were irradiated by a 1 kW "Katun" CO_2-laser in an atmosphere of various gases, i.e., argon, nitrogen, and air. Under given experimental conditions, the following materials were used as powder coatings: pure metals and nonmetals, prepared chemical compounds, i.e., carbides, borides, silicides, nitrides, and oxides, as well as certain mechanical mixtures which enter into a reaction during the heating. The powder materials had a particle dimensions range of 10–30 μm; a $\sim$100 μm thick layer was applied. Following their treatment with lasers, samples were subsequently annealed at a 200–750°C temperature for 4 h. Surface layers were examined by means of durometer analysis (PMT-3), optimal microscopy

("Neofot–2"), and X–ray phase analysis (the ADP–1 automated diffractometer and Cu$K\alpha$–radiation). The surface roughness was estimated using a model 251 profile recorder/–roughness indicator while the layers' wear resistance was examined in an UMT–1 friction machine. Under the sliding dry friction conditions, a disk–disk method was used while ShKh15 steel (60 HRC) was used as the counterdisk material.

It was established as a result of these experiments that the alloying process is rather critical to the laser radiation modes and conditions. With respect to the depth and quality of the alloyed layers, the best results were obtained with a 1.5–2.0 mm laser exposure spot and a scanning rate of 30–50 cm/min. If the laser radiation was defocused, resulting in an increase in the exposure spot, the alloying zone depth decreased while its homogeneity deteriorated and surface roughness rose. As the impact spot diameter increased further, no surface melting was observed although the powder layer was probably welded on to the sample.

Under optimal focusing conditions, the alloyed layer depth in the case of argon treatment varies insignificantly with the laser beam scanning rate within a 20–90 cm/min range. A 200–300 μm layer depth was attained for nonmetallic coatings, 300–400 μm for metals, and 400–500 μm for most chemical compounds. Moreover, the highest depth of 600 to 650 μm was obtained for boride–based coatings. Yet, as the scanning rate increased, the melting zone width decreased from 2.0 to 0.5 mm while the heat–affected area (ZTV) depth dropped from 500 to 200 μm. Such a difference in the laser–affected area dimensions is probably mostly related to the different optical and thermal properties of the powders used as well as the selected laser radiation mode. In most cases, the alloying zone was rather homogeneous due to the fact that there was a sufficiently complete mixing in the melt. Furthermore, the surface roughness quality was high. Thus, e.g., when alloying steel 5KhNM using W_2B_5 boride, the roughness parameter R_a was equal to 2.27 and 5.56 μm along and across the alloying track, respectively.

When a number of coatings ($HfSi_2$, W–C, ...) was used, there was no complete mixing in the alloying zone and large vortices of materials of various compositions were observed in the structure. This, as a rule, resulted in a higher surface roughness. Experiments carried out with a TiN powder ($\sim$200 μm) revealed that in this case, a peculiar composition structure was formed on steel Kh12F1. TiN inclusions with a 11,000–12,000 MPa microhardness were observed in this structure. In a general case, a finely disperse structure (Fig. 1), often cellular–dendritic in character, formed in the alloying zone.

Caption: Figure 1. Microstructure of steel 45 during laser alloying using VB_2: a and b – $\times$100 and 500, respectively. [Figure not reproduced]

It has been established that by using laser alloying of steel 45 and 5KhNM, one can increase the surface layer hardness to 11,500–12,000 MPa (70–72 HRC) and up to 10,000 MPa (67 HRC) when alloying steel Kh12F1. A high hardness level was attained in all brands of steel by using W and B as coatings. In steel 45, a considerable increase in hardness was also observed when using C, WC, TiB_2, WSi_2, and $TiSi_2$ powders. The values of microhardness of the hardened layers in the case of alloying steel 5KhNM are

summarized in the table below; one can see that the use of a broad range of alloying materials results in the surface layer hardening. Furthermore, a more than fourfold (20 to 90 cm/min) increase in the scanning rate had little effect on hardening. This can be attributed to the small change in the alloying zone depth but primarily to an increase in its width. Thus, under such conditions the alloying element concentration in the melt probably remained virtually unchanged. Yet, under higher scanning rates when using certain silicides, nitrides, and oxides as the alloying materials, alloying zone homogeneity deteriorated in the surface layer and pores of various sizes as well as small cracks appeared in that zone. It should be noted that deviations in the laser radiation's mode composition from optimal led to a change in the geometric dimensions of the alloying zone and worsened its properties.

Laser Alloying of Steel 5KhNM Using Various Powders

Material	*H*, MPa	Heat stability (60 HRC) *t*, °C	Comments
Si	7,500–10,500	350	
C	8,000–11,000	150	Pores
B	11,000–11,500	350	Pores, rough surface
W	9,000–11,000	550	Pores
Mo	7,500–9,000	550	
Al	7,700–8,000	150	
Ti	9,000–11,700	150	
Ni	7,400–10,000	550	Pores
Nb	3,300–4,700	–	Pores, rough surface
WC	5,500–8,300	150	Pores
T_aC	5,800–7,300	–	
HfC	8,000–9,000	150	
SiC	7,500–9,200	480	
B_4C	9,000–11,000	450	Pores
TaB	8,000–9,000	200	
HfB_2	5,000–9,000	150	
W_2B_5	9,000–12,000	600	
Co_3B	9,000–11,500	200	Pores, rough surface
VB_2	8,000–9,500	550	
TiB_2	9,000–11,500	450	
WSi_2	6,700–9,500	300	
$TiSi_2$	6,000–7,000	–	
TaSi	8,000–11,500	400	
VSi_2	7,000–9,000	300	Pores
$CoSi_2$	9,000–12,000	600	
$HfSi_2$	8,000–10,000	250	

Material	H, MPa	Heat stability (60 HRC) t, °C	Comments
VN	2,500–3,500	–	
AlN	10,000–12,000	175	
TiN	6,500–9,000	150	
TaN	6,000–11,500	200	Pores, cracks
Al_2O_3	9,500–11,500	150	Pores, rough surface
ZrO_2	6,000–7,000	–	Cracks, rough surface

We should note that for steel Kh12F1, the alloying zone hardness did not exceed 6,000 to 7,000 MPa (52–58 HRC) in most cases. Moreover, a considerable microhardness spread across the zone depth was observed. We know that during the heat treatment of steel Kh12 by laser, the microhardness does not exceed 4,000–4,500 MPa in the melt zone. Consequently, the microhardness can be increased somewhat in the melting zone during laser alloying. Yet, in most cases, the best hardening of steel Kh12F1 was attained in the ZTV (8,000–9,000 MPa).

It is also noted that an increased hardness was also observed in ZTV during the alloying of steel 45 and 5KhNM A high degree of hardening was observed, e.g., during the alloying of steel 5KhNM using VN, SiC, and $HfSi_2$ coatings. Such a hardness increase can be attributed to the diffusion of alloying elements into the ZTV. Thus, radiography research in [4] revealed that when steel is boronized with the help of a pulsed laser ($\tau_{имп} \sim 5$ ms), local boron penetration of the ZTV from the alloying zone can occur. This can be attributed to the fact that melting occurs primarily along grain boundaries which are penetrated by boron. Given laser alloying in the CW mode, the molten metal pool lifetime will be greater than that of pulsing modes by one or two orders of magnitude. In the final analysis, this creates the conditions for a more intensive frontal/diffusion ZTV penetration by alloying elements. It has been noted that the most uniform microhardness distribution in this zone is observed in samples hardened beforehand.

We know from [5, 6] that in the case of laser heat treatment, the structures' hardness is determined by an optimal combination of the solid solutions' saturation and concentration inhomogeneity. While during the laser heat treatment this phenomenon is attained by partial or complete dissolution of the carbides present in the source metal, in the case of laser alloying, one can also employ the hardening mechanism caused by an increase in the level of elastic distortions of the solid solutions' crystal lattice due to the discrepancy between the atomic dimensions of the solvent and the alloying element. Furthermore, it becomes possible to saturate the alloying zone additionally with carbide, boride, silicide, and other phases.

It was established by X-ray phase analysis that an iron–based solid solution may be considerably oversaturated with alloying elements with a concomitant precipitation of finely

disperse inclusions. When powdered pure substances, e.g., metals, (see table) were used, martensite structures were primarily formed in surface layers of steel 45 and 5KhNM; simultaneously, alloyed carbides and Mo_2C, WC, and W_2C carbides were formed. During the alloying of steel Kh12F1, a considerable amount of highly alloyed residual austenite was present in the structure.

We should note that during the treatment of powder layers even in an argon medium, alloying elements partially burned out, especially the nonmetals (B and C) during their interaction with residual air. The use of chemical compounds as coatings resulted in a more complicated alloying process kinetics. If chemical compound powders are heated by a laser, they may melt, decompose, and sublimate. Following a convective mixing with molten steel with subsequent crystallization, finely disperse source compounds as well as compounds based on the constituent elements formed in the structure in most cases. Thus, e.g., during the alloying of steel 5KhNM with the WSi_2, W_2B_5, and TiB_2 compounds, inclusions of source compounds as well as small amounts of α-W_2C, W; α-W_2C, WC; and Ti, B_4C, $Fe_{23}(C_9B)_6$ were observed in the structure alongside martensite.

In this experiment, we also examined characteristic features of laser alloying using mechanical mixtures. To this end, mechanical mixtures of W–Si, Ti–Si, B–C, Si–C, W–C, Ti–B, and W–B in stoichiometric ratios which corresponded to the WSi_2, $TiSi_2$, B_4C, SiC, WC, TiB_2, and W_2B_5 compositions were applied to the surface of steel 5KhNM. They were then treated in an inert atmosphere under the same conditions under which samples with chemical compounds applied to them were treated. It was established that the use of such mixtures as W–Si, Si–C, and Ti–B reduces the hardening effect as compared to compounds. Moreover, the surface layer quality deteriorated: pores and cracks appeared and surface roughness increased. In a number of cases, the alloying zone composition was less homogeneous. Thus, e.g., when the Ti–B mixture was used, inclusions whose microhardness reached 8,000–9,000 MPa were observed in the alloying zone whereas microhardness in the remaining part of the sample was below 6,000–8,000 MPa while in the some areas it dropped to 4,000 MPa. At the same time, when a TiB_2 powder was used for alloying, a sufficiently homogeneous structure with a more uniform microhardness distribution was observed; this structure had a greater stability to annealing.

In other cases, the hardening degree slightly depended on the type of coatings used. Moreover, the hardened layer's defects could be observed both in the case of chemical compounds and mechanical mixtures. Thus, pore formation was observed in the case of B_4C and W–C coatings while surfaces were very rough in the case of B_4C, Ti–Si, and W–B compositions. It has been noted that a good surface layer quality combined with a high hardness was observed when W_2B_5 boride was used as the alloying powder.

An analysis of the resulting data shows that in the case of laser alloying, thermochemical processes of the alloying elements' interaction among themselves as well as with substrate elements [7–9] are very important. When materials on an aluminum base produced by compacting mechanical mixtures (Al–Cu, Al–Ni, etc.) were treated, intensive pore formation was observed. At the same time, irradiation of materials which had the same chemi

cal composition but were obtained by alloyed powders ruled out the possibility of pore formation [7].

Similar results were obtained during the treatment of powder carbon steels [8] despite the fact they had an initial porosity of ~10–20%. Yet, in the case of irradiating materials on the basis of Fe + 2.5 mass % Cu + 0.5 mass % C, no pore "curing" occurred; on the contrary, porosity increased while branching pores and cracks reaching the surface [9] developed there. The surface layer decarburization in these experiments is attributed to the exothermic reaction of the interacting elements. If a violent exothermic reaction takes place in a small volume during a short time, a considerable quantity of heat is released. This leads to a local overheating of the melt, an evaporation of the material and, consequently, a bulk pore formation, an increase in roughness, and other surface layer defects [7].

We also examined characteristic features of the steel alloying in the case where air or nitrogen was fed to the treatment zone. When samples were irradiated in argon, a violent interaction reaction was observed only in the case of oxide powders. In this case, the sample surface was rather rough. In an atmosphere of air, most alloying materials applied to the surface burned out. Moreover, the surface layer quality deteriorated considerably. When steels were alloyed in an atmosphere of nitrogen, microhardness of steels 45, 5KhNM, and Kh12F1 in the melting zone reached 5,000–7,500, 8,000–8,500, and 3,500 to 5,500 MPa, respectively. Rather close values of hardness were attained during the alloying of steel using a ready TiN powder in an inert gas atmosphere. When alloying steel 45 with the AlN powder, the surface layer hardness amounted to 6,000–7,000 MPa, while in the case of treating samples with Al coatings in an atmosphere of nitrogen, it rose to 7,500–9,500 MPa.

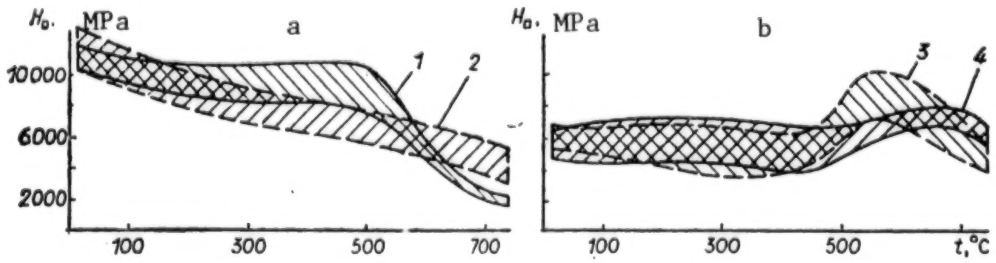

Fig. 2. Heat stability of steel 5KhNM (a) and Kh12F1 (b) in the case of alloying using various materials: *1* – W; *2* – B; *3* – TaC; *4* – WC.

Thus, when alloying elements which vigorously interact with nitrogen during heating are used, it is possible to saturate surface layers comprehensively. At the same time, it has been established that alloying of, e.g., steel 5KhNM with titanium in argon may lead to a considerable hardening effect: 9,000–11,700 MPa (65–71 HRC).

Subsequent annealing of the samples revealed that laser alloying of the steels under study makes it possible to increase their heat stability considerably (Fig. 2). The results of

heat stability studies of steel 5KhNM relative to the 60 HRC level are summarized in the table. One can see that when W, Mo, Ni, W_2B_5, VB_2, and $CoSi_2$ powders are used as coatings, the steel's high–temperature stability increases to 550–600°C. It is noted that as the annealing temperature increases, hardness decreases smoothly while the spread of its values along the alloying zone also decreases.

One can see that many alloying elements greatly affect the decomposition of martensite by slowing down the growth of carbide particles and preserving the α–solution's saturation with carbon. For example, additions of W, Mo, V, Co, and Si elements [10] contained in the powders used have this effect. The martensite decomposition delay can be attributed to a decrease in the carbon diffusion rate in the α–solution or to an increase in the interatomic bond strength in the α–solution lattice which complicates the atoms' transition across the α–solution/carbide boundary. This may also slow down the dissolution of small particles and delay the growth of large particles during the coagulation.

The hardness of alloyed layers of steel Kh12F1 had a more complicated variation pattern. When a number of alloying powders was used in the 550–650°C range, the layer's microhardness increased. For example, for TaC, microhardness reached the maximum value of ~10,000 MPa (68 HRC). We know that such an increase should be attributed to the decomposition of residual austenite and to secondary hardening. Since a large amount of $A_{ост}$ is observed in the structure of steel Kh12F1 following laser treatment, high–temperature annealing is accompanied by a carbide precipitation from residual austenite and a depletion of carbon and alloying elements. As a result, the martensite point $M_н$ rises and residual austenite becomes capable of undergoing a martensite transformation when it is cooled below the tempering temperature. Secondary hardening is caused by the formation of clusters from the atoms of the alloying elements and carbon and the transformation of relatively rough cementite particles which dissolve during heating into disperse deposits of special carbides of the W_2C, Mo_2C, VC, and TiC type [10].

Wear resistance tests reveal that laser alloying of surface layers makes it possible to increase wear resistance of steels considerably. When steel 45 is alloyed by, e.g., the WC carbide, its wear resistance under dry friction conditions increases by a factor of 2.5–3.

Bibliography

1. Rykalin, N. N., Uglov, A. A., Zuyev, I. V., Kakora, A. N. "Lazernaya i elektronnoluchevaya obrabotka materialov. Spravochnik" [Laser treatment and cathode ray machining of materials: A reference]. Moscow, 1985.

2. Leontyev, P. A., Khan, M. G., Chekanova, N. T. "Lazernaya poverkhnostnaya obrabotka metallov i splavov" [Metal and alloy surface treatment by lasers]. Moscow, 1986.

3. Kraposhin, V. S. ITOGI NAUKI I TEKhNIKI. SERIYa MiTO, 1987, vol. 21, pp. 144–206.

4. Lakhtin, Yu. M., Kogan, Ya. D., Buryakin, A. V. MiTOM, 1985, No. 11, pp. 9–11.

5. Brover, G. I., Varavka, V. N., Fedosiyenko, S. S. FiKhOM, 1988, No. 1, pp. 120–126.

6. Burakov, V. A., Brover, G. I., Burakova, N. M. MiTOM, 1985, No. 11, pp. 2–6.

7. Golubev, V. S., Yevstratenko, L. P., Laskovnev, A. P., Chebotko, I. S. VESTsI AN BSSR. SER. FIZ.-TEKh. NAVUK, 1988, No. 1, pp. 32–36.

8. Blinovskiy, V. A., Pustovoyt, V. N., Shugay, K. K. "Tezisy dokladov soyuznoy nauchno-tekhnicheskoy konferentsii 'Novyye materialy i tekhnologii termicheskoy obrabotki metallov'" [Proceedings of the national scientific and engineering conference on "New Materials and Technologies for the Heat Treatment of Metals"]. Kiev, 1985, pp. 185–187.

9. Kovrigin, V. A., Goryushin, M. N., Dubrovskiy, S. V., *et al.* MiTOM, 1984, No. 7, pp. 27–29.

10. Novikov, I. I. "Teorita termicheskoy obrabotki metallov" [The theory of the heat treatment of metals]. Moscow, 1986.

COPYRIGHT: Vydavetstva "Navuka i tekhnika" Vestsi AN BSSR, seryya fizika-tekhnichnykh navuk, 1989

UDC 620.17:669.295:621.78.014

Hardening of VT23 Titanium Alloy With Orthorhombic Martensite Structure During Rapid Heating

907D0092B Minsk IZVESTIYA AKADEMII NAUK BELORUSSKOY SSR: SERIYA FIZIKO-TEKHNICHESKIKH NAUK in Russian No 4, Oct-Dec 89 (manuscript received 6 Jul 88) pp 26-30

[Article by V. V. Ivashko and N. I. Krino, Engineering Physics Institute at the Belorussian Academy of Sciences]

[Text] Orthorhombic α''-martensite [1, 2] forms in titanium alloys containing 4-8% molybdenum or other β-isomorphic elements in an equivalent amount during the quenching starting at β-phase temperatures. It is known [1-7] that α''-martensite is unstable to subsequent thermal or mechanical exposures. It was shown in [1, 4, 7] that following a tempering at temperatures of 400-600°C, decomposition processes occur with the formation of a finely disperse β-phase particles. The authors of [8, 9] established that the decay of orthorhombic martensite occurs not only during isothermal heating, but also under rapid heating conditions. It was established using the electric resistance method that α''-martensite may become converted to the β-phase without diffusion; this phase then decays by the conventional diffusion mechanism. The hardening processes occurring during the decay of α''-martensite under rapid heating conditions are less known. Consequently, the goal of this research was to examine the effect of the initial structural state of α''-martensite and the rate of subsequent heating on the efficacy of electrical and thermal hardening of titanium alloys with an α''-martensite structure as well as the related phase and structural transformations.

We examined samples cut from VT23 alloy sheets. The alloy had the following chemical composition (in % by mass): Al - 4.8; V - 4.3; Mo - 2; Cr - 1.1; Fe - 0.5; Zr - 0.04; C - 0.02; Si - 0.03; N - 0.015; O - 0.150; H - 0.01; Ti - the remainder. 5.6 mm-thick sheets were obtained by rolling at $(\alpha+\beta)$-phase temperatures. After the rolling, the sheets were annealed at 750°C. The samples were cut from the sheets in a direction perpendicular to the rolling direction and were heated - by passing electric current through them - at a rate of 100°C/s to 950 and 1,100°C, then quenched in water. In order to attain bulk hardening, the quenched samples were heated again to 100-800°C at a rate of

10, 100, and 500°C/s, as well as in a furnace during 0.5 and 6 hours, then cooled in water. The structure and phase composition were examined by the electron microscopy and X-ray analysis methods. Tensile tests were carried out in 25 mm-long samples with a 5 mm working part diameter.

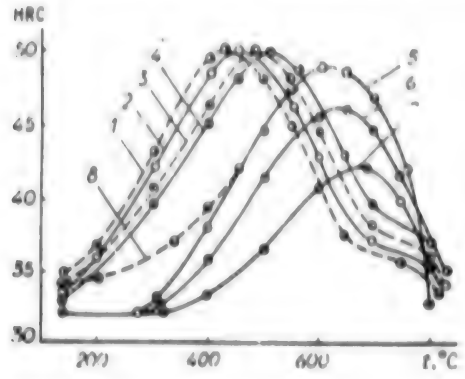

Fig. 1. Effect of heating conditions for quenching and subsequent aging on the VT23 alloy's hardness: heating for quenching: *1*, *3*, *8* – $t_{зак}$ = = 1,100°C, $V_н$ = 100°C/s; *2*, *4*, *5*, *6*, *7* – $t_{зак}$ = = 950°C/s, $V_н$ = 100°C/s. Aging: *1*, *2* – 6 h; *3*, *4* – 0.5 h; *5*, *8* – 10°C/s; *6* – 100°C/s; *7* – 500°C/s.

The hardness measurement results shown in Fig. 1 reveal that a quenched VT23 alloy is effectively hardened both in the case of furnace and rapid heating. After being heated in a furnace at 200°C during 6 h, the hardness of an alloy quenched at 950°C rises from 32 to 33 HRC in the initial state to 36–37 HRC. As the temperature rises to 400°C, hardness increases to 48 HRC. At 450°C, the alloy's limit of hardness is 50 HRC. A subsequent temperature increase to 600–700°C is accompanied by a uniform hardness decrease to 42 and 37 HRC, respectively.

Thus, the quenched alloy's principal hardening related to the decay of α''-martensite and a hardness increase from 37 to 50 HRC develops within the 200–450°C range. An exposure shortening to 30 min during the heating shifts the hardening/softening processes 30 to 50°C upward along the temperature scale. The maximum hardness level is attained after a heating to 500°C and is equal to 50 HRC.

If moderate heating rates (10°C/s) are used, hardening processes are shifted 150°C upward relative to the curves obtained after a 6 h heating. Under such heating conditions, the maximum value of hardness at 600°C is 49 HRC. As the heating rate rises to 100 and 500°C/s, the temperature range within which the main hardening occurs shifts upward by 200 and 250°C whereas the loss of strength processes occur virtually within the same 700–800°C range for the 10, 100, and 500°C/s rates. We should note that under high heating rate conditions, a quenched alloy does not reach the hardening level limit. When heated at a 100°C/s rate, the maximum hardness is 46 HRC while when heated at 500°C/s – 42 HRC.

A study of mechanical properties shows that given a furnace heating to 200°C and a 30 min exposure, the strength and ductility characteristics of an alloy quenched at 950°C are preserved and maintained at a level of σ_b = 1,100–1,150 MPa, δ = 6%, and φ = 5%. A 300–400°C heating is accompanied by the hardening of the alloy while at 400–550°C it becomes embrittled within the 550–650°C interval. If the alloy is heated at a 500°C/s

rate, there is no embrittlement within this temperature range. The strength level limit is 1,300–1,400 MPa while the ductile properties remain at the level of the original quenched state ($\delta = 3$–5% and $\varphi = 4$–6%).

The VT23 alloy quenched beforehand at 1,100°C has a low yield point and is sufficiently ductile ($\sigma_b = 1{,}200$ MPa, $\sigma_{0.2} = 650$ MPa, $\delta = 15$–17%, and $\varphi = 28$–35%). Under furnace heating conditions, the yield strength rises from 830–850 MPa at 200°C to 1,100 MPa at 300°C. As the heating rate increases to 10°C/s, the mechanical properties of alloy heated to 100–300°C remain virtually unchanged. The yield point rises within the 300–500°C range. After a heating to 400–500°C, the yield strength is equal to 1,070–1,400 MPa, respectively.

Electron microscopy and X–ray structural analyses of the samples show that when an alloy is in a state quenched at 950°C, its structure represents α''–martensite and the residual β–phase. Following an additional heating, the α''–martensite decay degree was estimated by the X–ray structural method by measuring the angle between the α''–phase's (130) and (200) lines. It was established that following a heating to 100–300°C and an exposure for 6 h, the angle between the lines decreases gradually from 62 to 50 min (Cu emission). The angle decreases sharply within the 400–450°C interval. At 525°C, both of the α''–martensite's lines virtually merge into a single (110) line of the α''–martensite's $\alpha'(\alpha)$–phase.

During the rapid heating, martensite decays intensively within the 500–650°C range. As the α''–martensite line duplication disappears, weak responses of the β–phase's (200) line appear. When heated in a furnace for 6 h, the β–phase's appearance is observed at 500°C. When the heating time is shortened to 30 min, the temperature at which the β–phase's diffraction lines are recorded rises to 550°C. The appearance of diffraction β–lines under continuous heating conditions at 10 and 100°C/s rates is recorded after the alloy is heated to a temperature of 635 and 660°C, respectively.

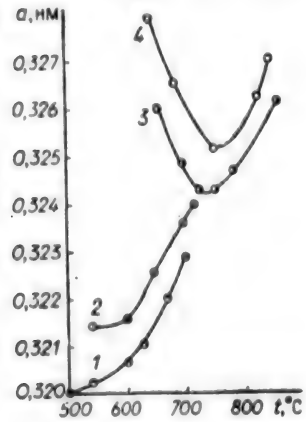

Fig. 2. Variations in the β–phase lattice parameter as a function of the aging conditions of a hardened VT23 alloy ($t_{зак} = 1{,}100$°C, $V_н = 100$°C/s. The aging conditions are : *1*, *2* – 6 and 0.5 h; *3*, *4* – 10 and 100°C/s, respectively.

The results of measuring the β–phase crystal lattice constant shown in Fig. 2 indicate that as the furnace temperature rises from 500 to 700°C, the β–phase crystal lattice con-

stant increases to 0.323 and 0.3235 nm given a furnace exposure of 6 h and 30 min, respectively. Moreover, variations in the spacing between the planes are insignificant within the 500–600°C range while the intensive growth related to the depletion of chromium and vanadium from the β–phase occurs about 600°C. The β–phase crystal lattice variations display a different pattern in the samples which underwent decay under rapid heating conditions. Within the 600–750°C range, the β–phase lattice constant decreases from 0.326 and 0.328 nm to 0.324 and 0.325 nm, respectively, given a heating rate of 10 and 100°C/s, and increases during a subsequent heating from 750 to 800°C. By analyzing the integrated intensity of $(200)_\beta$ diffraction lines, it was established that the maximum amount of the β–phase forming during the α"–martensite decay under rapid heating corresponds to a temperature of 750°C. As the heating rate increases from 10 to 100°C/s, the β–phase content by volume fixed by quenching at a 750°C temperature decreases.

Discussion of the Results. We know that alloys, heated in a furnace at 1,100°C and quenched for the α"–phase, decay during the aging and form a spinodal structure [1]. In our case, no such structure is identified since α"–martensite is distinguished by a high level of defects and chemical inhomogeneity. After being quenched at temperatures close to the α→β–transformation boundary, the yield strength increases while the ductile characteristics decrease sharply. One can speculate that α"–martensite undergoes partial decay during the quenching or that the omega–phase is being fixed. Yet the results of X–ray structural and electron microscope analyses do not corroborate these assumptions.

After the heating at a rate of 10°C/s to 100–500°C, recrystallized β–grains with 3–10 μm dimensions are observed in the alloy structure. Finely disperse formations whose origin has not been ascertained appear on electrone microscope pictures taken along the boundaries and inside the β–grains. We should note that at this decay stage, the strength level and yield strength increase sharply. Acicular martensite or twins do not form in the alloy structure following such a treatment whereas α"–martensite is clearly recorded by X–ray photography. This factor is attributed to the development of an α"→β–transformation during the electrolytic foil preparation [2].

Twinned α"–martensite, which is sufficiently stable up to 100–300°C during the rapid heating is recorded in the samples quenched at 1,100°C. If the phase composition variations are estimated by the results of the X–ray analysis, twinned martensite under rapid heating conditions is preserved up to 450–500°C without noticeable changes. According to electron microscope research data, homogeneous decay accompanied by an increase in the strength level and yield strength occurs inside twinned martensite laminae within the 300–500°C range.

During the subsequent rapid heating above 500°C, the mechanism and decay kinetics of metastable phases and the hardening character of the samples quenched at 950 and 1,100°C are virtually the same. Within the 550–650°C range, the α"–martensite's stratification into zones enriched with and depleted of β–alloying elements intensifies sharply. In the zones depleted of β–stabilizers, the crystal lattice's rhombic distortion decreases. After the alloy has been heated to 600–650°C, acicular crystals of hexagonal α′–martensite appear in its structure. In the zones enriched with β–stabilizers, the first formations

of the β–phase are observed; in these zones, the β–alloying element concentration is below the equilibrium typical of a given temperature under furnace heating conditions. We should note that as acicular α'–martensite appears in the structure, it becomes embrittled (σ_b = 1,200–1,600 MPa, $\delta \leq 1\%$, $\varphi \leq 1\%$).

Within the 650–750°C range, α'–martensite decay processes accompanied by an increase in the volume content of the β–phase and a disordering of the alloy occur. A thinly laminated ($\alpha + \beta$)–structure is formed. The α–phase represents 0.1 μm–thick and 1–2 μm–long laminae in which twins and individual dislocations are observed. As the temperature increases to 750°C, the β–phase's chemical composition approaches an equilibrium. A highly–developed interface and the presence of internal defects facilitate an intensive development of an $\alpha \rightarrow \beta$–phase transformation within the 750–800°C interval; after an 800°C quenching, this transformation insures the fixing of the α''–martensite enriched with β–stabilizers. Residual α– and β–phases are recorded simultaneously with α''–martensite by X–ray structural analysis. As α''–martensite appears, the VT23 alloy loses strength to 1,100 MPa while its ductile properties rise to δ = 10–12% and φ = 25–30%.

Summary

1. The hardening and loss of strength processes as well as the related structural and phase transformations occurring during the decay of orthorhombic martensite in sheets of the VT23 titanium alloy under rapid continuous heating conditions have been examined. It is shown that the maximum values of hardness are attained within the 550–650°C temperature range.

2. It was established that the use of rapid heating rates (10–500°C/s) during aging is accompanied by a shift of the hardening processes 150–250°C relative to the relationships obtained under furnace heating conditions. It was shown that the hardening during the α''–martensite's decay is related to the diffusion processes of the β–stabilizer redistribution, as well as the formation of hexagonal α'–martensite and finely disperse β–phase formations.

Bibliography

1. Davis, R., Flower, H. M., and West, D. R. F. // Acta Metallurgica, 1979, vol. 27, pp. 1041–1052.

2. Trenogina, T. G., Vozilkin, V. A., Zverev, Z. F., Meshchaninov, L. S. FIZIKA METALLOV I METALLOVEDENIYe, 1986, vol. 61, No. 1, pp. 153–155.

3. Lyasotskaya, V. S., Frolova, T. F., Mamonova, F. S. IZVESTIYa VUZOV. TsVETNAYa METALLURGIYa, 1977, No. 5, pp. 129–134.

4. Kolachev, B. A., Mamonova, F. S., Lyasotskaya, V. S. IZVESTIYa VUZOV. METALLY, 1974, No. 1, pp. 200–203.

5. Yermolova, M. I., Zhebyneva, N. F., Solonina, O. P., Ovchinnikova, G. V. FIZIKA METALLOV I METALLOVEDENIYe, 1982, vol. 53, No. 4, pp. 738–743.

6. Maltsev, M. V., Kashnikov, N. I. FIZIKA METALLOV I METALLOVEDENIYe, 1977, vol. 43, No. 6, pp. 1259–1264.

7. Yermolova, M. I., Bezgina, V. I., Karpova, I. G., *et al.* FIZIKA METALLOV I METALLOVEDENIYe, 1982, vol. 53, No. 6, pp. 1153–1160.

8. Ivanov, A. S., Tomsinskiy, V. S. IZVESTIYa AN SSSR. METALLY, 1974, No. 5, pp. 173–179.

9. Ivasishin, O. M., Kovalevskiy, A. V., Krivenko, V. I., Oshkaderev, S. P. "Voprosy metallovedeniya stali i titanovykh splavov" [Physical metallurgy issues: Steel and titanium alloys]. Perm, 1978, pp. 120–125.

COPYRIGHT: Vydavetstva "Navuka i tekhnika" Vestsi AN BSSR, seryya fizika–tekhnichnykh navuk, 1989

UDC 621:544.55

Calculating Characteristics of Solidification of Steel Ingot in Mold With Convection Heat Exchange of Liquid Core, Two-Phase Zone

907D0039A Minsk DOKLAY AKADEMII NAUK BSSR in Russian Vol 33 No 9, Sep 89 (manuscript received 14 Dec 88) pp 811-814

[Article by P.V. Sevastyanov, V.I. Timoshpolskiy, V.N. Bobrov and E.A. Gurvich, Byelorussian Polytechnical Institute: "Calculating the Characteristics of Solidification of a Steel Ingot in a Mold With Convection Heat Exchange of a Liquid Core and a Two-Phase Zone"; presented by G.A. Anisovich, member of the Academy of Sciences of the Byelorussian SSR; the first two paragraphs are a source-supplied English summary]

[Text] The paper deals with a calculation procedure to be used for steel ingot solidification based on a special coordinate transformation which makes it possible to stabilize the dimensions of solid, liquid and two-phase zones in the ingot. If necessary, it is also possible to use the stationary irregular steps for these zones.

The procedure was tested in the calculation of ingot solidification in a cast-iron mold, and the calculation results showed good agreement with experimental data.

Models based on descriptions of solid, liquid and two-phase zones of an ingot by a single heat conduction equation with variable coefficients are often used in calculations [1]. In the liquid core, an effective thermal conductivity coefficient is used in expressions which implicitly reflects convective mixing of the melt and for this reason sometimes takes values that are greater by an order of magnitude than the heat conductivity of stationary melt. This artificial technique, in our opinion, leads the model too far from the physical reality and prevents it from providing the appropriate accuracy.

Since temperature gradients in the liquid core do not exceed a few degrees because of intensive mixing [1], it appears that a model more representative of the actual physics of the process would be one where the liquid core is

treated as a coherent entity, with average temperature of its own, engaged in heat exchange with the two-phase zone according to the convection law. However, such a model requires defining the positions of liquidus isotherms explicitly. This is impossible with conventional methods, where the spatial position of the two-phase zone is determined after temperature calculations.

In this context, we employed a technique based on a special transformation of the coordinates of the calculation region so as to build a model of solidification with convection heat exchange of the liquid zone and the two-phase zone. We consider solidification of a flat ingot with thickness $2H_1$ in a cast iron mold of a thickness H_2. To make calculations more convenient, we place the origin of coordinates on the outer surface of the ingot.

We will identify the solid two-phase and liquid zones of the ingot by indices 1, 2 and 3, respectively. We now can write the mathematical model:

[=1]

$$\rho(T_1)C(T_1)\frac{\partial T_1}{\partial \tau} = \frac{\partial}{\partial x}\left(\lambda(T_1)\frac{\partial T_1}{\partial x}\right),\ 0 \leqslant x \leqslant \xi_{c1}(\tau); \tag{1}$$

$$\rho(T_2)C(T_2)\frac{\partial T_2}{\partial \tau} = \frac{\partial}{\partial x}\left(\lambda(T_2)\frac{\partial T_2}{\partial x}\right),\quad \xi_{c2}(\tau) \leqslant x \leqslant \xi_{\pi}(\tau); \tag{2}$$

$$\rho(T_3)C(T_3)\frac{dT_3}{d\tau} = \frac{\alpha_1(T_{\pi}-T_3)}{H_1-\xi_{\pi}(\tau)};\quad \xi_{\pi}(\tau) \leqslant x \leqslant H_1; \tag{3}$$

$$\rho_1(U)c_1(U)\frac{\partial U}{\partial \tau} = \frac{\partial}{\partial z}\left(\lambda_1(U)\frac{\partial U}{\partial z}\right);\ 0 \leqslant z \leqslant H_2; \tag{4}$$

$$\lambda(T_1)\frac{\partial T_1}{\partial x}\bigg|_{x=0} = \sigma_1(T_1^4-U^4)+\alpha_{\kappa}(T_1-U); \tag{5}$$

$$\lambda(T_1)\frac{\partial T_1}{\partial x}\bigg|_{x=\xi_{c1}(\tau)} = \lambda(T_2)\frac{\partial T_2}{\partial x}\bigg|_{x=\xi_{c1}(\tau)}; \tag{6}$$

$$T_1|_{x=\xi_{c1}(\tau)} = T_2|_{x=\xi_{c1}(\tau)} = T_c; \tag{7}$$

$$\lambda(T_2)\frac{\partial T_2}{\partial x}\bigg|_{x=\xi_{\pi}(\tau)} = -\alpha_1(T_{\pi}-T_3);\ T|_{x=\xi_{\pi}(\tau)} = T_{\pi}; \tag{8}$$

$$\lambda_1(U)\frac{\partial U}{\partial z}\bigg|_{z=0} = -\sigma_1(T_1^4-U^4)-\alpha_{\kappa}(T_1-U); \tag{9}$$

$$\lambda_1(U)\frac{\partial U}{\partial z}\bigg|_{z=H_2} = -\sigma_2(U^4-T_{cp}^4)-\alpha_2(U-T_{cp}); \tag{10}$$

$$T_1|_{\tau=0} = T_2|_{\tau=0} = T_3|_{\tau=0} = T_0;\ U|_{\tau=0} = U_0, \tag{11}$$

where T and U are the temperature in the ingot and in the mold; α_1 and α_2 are the coefficients of convection heat exchange of liquid and two-phase zones of the mold and the environment with temperature T_{cp}; α is the contact heat

exchange coefficient in the gap between the ingot and the mold which describes the thermal conductivity of the gap; σ_1, σ_2 are coefficients of radiation in the gap and on the outer surface of the mold; T_l and T_c are the liquidus and solidus temperatures, respectively; and ρ, c and λ are the density, heat capacity and heat conductivity of the material, respectively. The release of hidden melting heat is taken into account implicitly in the temperature relationship of specific heat conductivity $c(T_c)$ in the two-phase zone. In order to obtain full closure of system (1)-(11) we must add equations describing the dynamics of liquidus front $\xi_l(\tau)$ and solidus front $\xi_c(\tau)$. Before doing this, we rearrange the system by introducing new coordinates

$$[\ =l] \qquad \eta_1 = \frac{x}{\xi_c(\tau)}, \quad 0 \leqslant x \leqslant \xi_c(\tau); \tag{12}$$

$$\eta_2 = \frac{x - \xi_c(\tau)}{\xi_{cl}(\tau) - \xi_c(\tau)}, \quad \xi_c(\tau) \leqslant x \leqslant \xi_{cl}(\tau). \tag{13}$$

Passing to the new coordinates and reducing the notation by omitting the temperature dependencies of the thermophysical properties, we obtain

$$[\ =l] \qquad \rho c\left(\frac{\partial T_1}{\partial \tau} - \eta_1 \frac{d\xi_c}{d\tau} \frac{\partial T_1}{\partial \eta_1} \frac{\partial \eta_1}{\partial x}\right) =$$

$$= \left(\frac{\partial \lambda}{\partial T}\left(\frac{\partial T_1}{\partial \eta_1}\right)^2 + \lambda \frac{\partial^2 T_1}{\partial \eta_1^2}\right)\left(\frac{\partial \eta_1}{\partial x}\right)^2; \tag{14}$$

$$\rho c\left(\frac{\partial T_2}{\partial \tau} + \left((\eta_2 - 1)\frac{d\xi_c}{d\tau} - \eta_2 \frac{d\xi_{cl}}{d\tau}\right) \frac{\partial T_2}{\partial \eta_2} \frac{\partial \eta_2}{\partial x}\right) =$$

$$= \left(\frac{\partial \lambda}{\partial T}\left(\frac{\partial T_2}{\partial \eta_2}\right)^2 + \lambda \frac{\partial^2 T_2}{\partial \eta_2^2}\right)\left(\frac{\partial \eta_2}{\partial x}\right)^2; \tag{15}$$

$$\lambda \frac{\partial \eta_1}{\partial x} \frac{\partial T_1}{\partial \eta_1}\bigg|_{\eta_1 = 0} = \sigma_1(T_1^4 - U^4) + \alpha_{\text{к}}(T_1 - U); \tag{16}$$

$$\frac{\partial \eta_1}{\partial x} \frac{\partial T_1}{\partial \eta_1}\bigg|_{\eta_1 = 1} = \frac{\partial \eta_2}{\partial x} \frac{\partial T_2}{\partial \eta_2}\bigg|_{\eta_2 = 0}; \tag{17}$$

$$T_1|_{\eta_1 = 1} = T_2|_{\eta_2 = 0} = T_c; \ T_2|_{\eta_2 = 1} = T_{\text{л}}; \tag{18}$$

where

$$\frac{\partial \eta_1}{\partial x} = \frac{1}{\xi_c(\tau)}; \quad \frac{\partial \eta_2}{\partial x} = \frac{1}{\xi_{cl}(\tau) - \xi_c(\tau)}.$$

The remaining equations of system (1)-(11) are not changed. We expand T_2 as a series in the neighborhood of $\eta_2 = 0$, leaving terms above the second infinitesimal order:

$$T_2(h_2, \tau) = T_2(0, \tau) + h_2 \frac{\partial T_2(0, \tau)}{\partial \eta_2} + \frac{h_2^2}{2} \frac{\partial^2 T(0, \tau)}{\partial \eta_2^2}. \tag{19}$$

From (18) it follows that $T_2(0,\tau) = T_c$. Expressing the second term in the right-hand side of (19) from (17) and the third term from equation (15) taken at $\eta_2 = 0$ and substituting these expressions into (19), we write the equation for

$$\frac{d\xi_c}{d\tau} = -\frac{\partial\lambda}{\partial T_2}\ \frac{q}{\lambda c\rho} + \frac{2\lambda}{\rho c q_c h_2(\xi_\pi - \xi_c)}\left(q_c - \lambda\ \frac{T_2(h_2,\ \tau) - T_c}{h_2(\xi_\pi - \xi_c)}\right), \tag{20}$$

where $q_c = \lambda\ \dfrac{\partial T_1}{\partial \eta_1}\ \dfrac{\partial \eta_1}{\partial x}\Big|_{\eta_1 = 1}$.

It is convenient to take for h_2 the step of the finite-element grid in the zone $0 \le \eta_2 \le 1$ near $\eta_2 = 0$; q_c is determined at each time step from solution of the thermal problem.

Likewise, expanding T_π as a series in the neighborhood of $\eta_2 = 1$, we write

$$\frac{d\xi_\pi}{d\tau} = \frac{\partial\lambda}{\partial T_2}\ \frac{q_\pi}{\lambda c\rho} + \frac{2\lambda}{\rho c q_\pi h_2(\xi_\pi - \xi_c)}\left(q_\pi - \lambda\ \frac{T_2(-h_2\tau) - T_\pi}{h_2(\xi_\pi - \xi_c)}\right), \tag{21}$$

where $q_l = \alpha_1(T_2 - T_l)$.

Equations (20) and (21) close the system and allow us at each time step to determine explicitly the boundary of the two-phase zone. The resulting conjugate system of partial derivative differential equations and ordinary differential equations (20) and (21) was solved by combining implicit difference schemes and a modified Euler method.

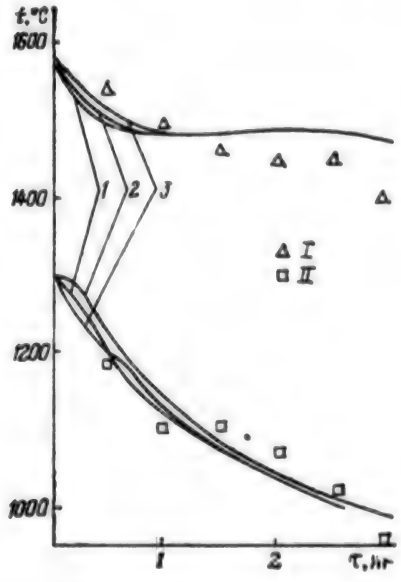

Figure 1. Temperatures measured at the center (*I*) and on the surface of an ingot (*II*): *1-3* — calculations for $\alpha_1 = 5000$; $\lambda_2 = 200$; $\alpha_1 = 1500$.

Figure 1 presents the result of a comparison of calculations with this method for various α_1 and calculations with a conventional model using effective thermal conductivity coefficient in a liquid core (curve *2*). The results were compared with experimental data on solidification of a blooming ingot from steel 45. The match of the results of the different models confirms that this calculation method is viable. The discrepancy between calculated and experimental data at $\tau > 1.5$ hr is due to the fact

that for a blooming ingot a one-dimensional model is a rough approximation.

The method has another important advantage over the conventional technique. In the new coordinates η_1 and η_2 the boundaries of the zones are stationary. This makes it possible to introduce, in isolated, regions stationary uneven grids which become denser at locations of nonlinearities, for example, near $\eta_2 = 1$, i.e., near the liquidus where most of the phase transition heat is released.

Bibliography

1. Samoylovich, Yu.A., Krulevetskiy, S.A., Goryainov, V.A., and Kabakov, Z.K., TEPLOVYE PROTSESSY PRI NEPRERYVNOM LITYE STALI [Thermal Processes During Continuous Steel Casting], Moscow, 1982.

UDC 621.762.3.001.6

Experience Manufacturing Parts From Metal Powders at "NKMZ" Production Association

907D0076A Moscow KUZNECHNO-SHTAMPOVOCHNOYE PROIZVODSTVO in Russian No 11, Nov 89 pp 27-28

[Article by V. P. Khalyuzin: "Experience Manufacturing Parts from Metal Powders at the "NKMZ" Production Association"]

[Text] Powder metallurgy is a young, but extremely important branch of modern technology. Modern cutters made of hard alloys produced by powder metallurgy method have caused a genuine revolution in metal cutting and in mining. Various cermet structural materials, as well as porous bearings, filters, and other items are being successfully used in industry.

The main advantage of powder metallurgy is that it is waste-free. Machining is eliminated, and the metal utilization factor doubles.

The "NKMZ" [Novokramatorsk Machine Building Plant] Production Association is making extensive use of iron graphite bushes, roller shafts, and other items. The reliable performance of cermet bushes installed on plant equipment instead of bronze and iron ones made it possible to begin research on the use of metal powder parts on new machinery and assemblies being designed.

Since 1975, cermet products have been widely used on rolling, metal ore mining, and other equipment produced at the plant and have been ordered by other enterprises. In the 11th Five-Year Plan this permitted the production of about 525 tons of cermet items, and the shop's annual output in 1988 rose to 150 tons. The production shop is equipped with two set of presses and gauging molds and is operated by 12 people.

Tests were performed on the serviceability of cermet roller shafts that replaced iron ones in rotary wheels of walking excavators and cermet bushes in shaft hoist brake systems. Experiments proved that under active loads cermet parts in excavators and shaft hoists demonstrated high serviceability and wear resistance.

Bronze and iron bushes had previously been installed on these machines. They were unreliable and their servicing required increased operating expenses. The strength characteristics of cermet bushes surpass those of bronze and iron ones. An important property of the cermet bushes is their high strength

characteristics, a 2-3-times lower friction coefficient at the same bearing assembly friction surface speeds, and self-lubrication with the oil in the parts' pores.

Experiments established that under active loads cermet bushes in shaft hoist brake beams, labyrinth bushes for roller bearings in rotary complexes, shafts for walking excavator rollers, and mixer bushes demonstrated high serviceability and wear resistance. The results of this work made it possible to replace 168 bushes of six kinds weighing a total of 300 kg on one shaft hoist and 224 rotary wheel roller shafts on one walking excavator. This produced an economic effect of more than 100,000 rubles per year, about 200 tons of iron on the roller shafts of excavator rotary wheels alone, not counting the savings from the extended service life of cermet parts.

A unique feature of the rolling mill transport machinery is that it is full of friction assemblies. The use of self-lubricated iron-graphite bushes simplifies the design and servicing of friction assemblies and makes it possible to save costly and scarce nonferrous metals. For example, iron graphite bushes were pressed into drag chain rollers on a strip conveyor on the 2300/1700 mill (strip weight 10 tons, transportation speed 0.5-1 m/sec, strip temperature 800-900°C). The conveyor demonstrated good performance qualities. Iron-graphite bushes were also provided in the rolls of the hot coil conveyor drag chain (coil weight to 2 tons),

On the wide strip mill sheet release, a sheet moving on the rollers is released into a pocket. The release has about 1,000 rollers. It was not difficult to lubricate this number of rollers. Releases with iron-graphite bushes operate on many continuous and semi-continuous hot rolling mills without additional lubricant.

Iron-graphite bushes are widely used in transport table assemblies. The tables are arranged in several rows next to one another, bearing are hard to reach, and it would be difficult to lubricate ordinary bushes. Another example of the use of cermet bushes in table rollers is the hot coil conveyor transfer sections.

Replacing bronze bushes with cermet ones doubled the service life of mixer roll bearings made at the plant, eliminated the need to lubricate them, and saved 15,000 rubles.

The distinguishing features of the manufacture of cermet products at this plant compared to other plants is their large overall dimensions and the individual nature of production (parts weighing up to 15 kg and dimensions to 300 mm).

To ensure cost-effective manufacture (particularly equipment payback) in small-series production, an enterprise standard was developed to ensure production of cermet bushes in 26 dimensional series from 20 to 220 mm in diameter. Standardized assemblies are used when different machines are designed.

Moreover, specialized cermet bushes cannot be replaced by other materials.

For example, unique bushes weighing 13 kg and measuring 250 x 280 mm in diameter were installed in the brake systems of new twin-drum shaft hoists. This made it possible to ensure their reliable operation, since bushes of other materials require lubricant which may fall onto the brake drums.

Measures are now being taken to expand the applications of powder metallurgy products and to use them not only as an anti-friction material, but also as a structural material.

Together with Kramatorsk NIIPTMASh [Scientific Research, Design, and Production Institute for Machine Building], we researched the replacement of copper conductor inserts for semi-automatic welders with cermet inserts, which permitted a fivefold increase in their durability and the replacement of No. 211 roller bearings in rolling equipment with bronze-graphite sliding bearings, which made it possible to change the design of rollers on TLS-3600 conveyors and save about 100,000 rubles, save more than 100 tons of metal, and free up more than 100,000 ball bearings. We also studied the materials and developed a process for manufacturing face milling cutter blade rods by hot compaction method. Given an annual demand of 560,000 rods, the introduction of this work will substantially lower the labor required to manufacture them.

The association is now taking steps to develop a hot compacting line in the powder metallurgy bay at KPTs-1 and to provide modern equipment. This will make it possible to expand output from 150 to 300 tons.

COPYRIGHT: Izdatelstvo, "Kuznechno-shtampovochnoye proizvodstvo"

UDC 621.777.07(088.8)

Producing Items With Specified Surface Hardness Distribution by Hydraulic Extrusion Method

907D0074A Moscow KUZNECHNO-SHTAMPOVOCHNOYE PROIZVODSTVO in Russian No 9, Sep 89 pp 10-11

[Article by Ya. Ye. Beygelzimer, V. N. Lagutin, A. H. Martynov: "Producing Items with Specified Surface Hardness Distribution by Hydraulic Extrusion Method"] -- For Official Use Only

[Text] When items are produced by hydraulic extrusion, hardness must sometimes be increased on certain segments of the surface of these items. This can be done by increasing overall product hardness, but hydraulic extrusion pressure rises. There is another way to solve this problem based on the redistribution of metal flows at the strain site.

This work describes the structure and method for manufacturing a die in which metal flows are controlled by the specified distribution of the height of the parallel along the perimeter of the die[1].

Segments with a higher parallel ensure greater resistance to metal motion and, according to the law of least resistance, smaller metal flows are directed into the corresponding areas.

Let us derive an equation for determining the length of the generatrices of the finishing portion of the die. According to reference 2, drawing stress is found with the formula:

$$\sigma_p = \kappa'(1 + \mu \operatorname{ctg} \alpha) \ln (F/f) + \chi\mu\kappa'(l/d), \quad (1)$$

where σ_p is drawing stress; κ', the metal's yield limit; μ, the coefficient of friction between the metal and the die; α, half of the angle of the entry part of the die; d, item diameter (when a profile is being draw, d is the diameter of the circle whose area equals the profile's cross section area); χ, a coefficient dependent on strain conditions.

Since there is no friction against the walls of a container in hydraulic extrusion, then according to reference 3 formula (1) can be used to calculate hydraulic extrusion pressure p:

$$p = \kappa'(1 + 0.1 \operatorname{ctg} \alpha) \ln (F/f) + 0.4\kappa'(l/d), \quad (2)$$

This formula assumes[2] that χ=4 and μ=0.1.

Let us present this formula in the form

$$\ln (F/f) = [p - 0.4(l/d)\kappa']/\kappa'(1 + 0.1 \operatorname{ctg}\alpha). \quad (3)$$

We apply equation (3) not to the entire body of the metal, but only to the surface layer, where F_1 and f_1 are the initial and final cross sections of this layer.

In this case equation (3) takes the following form:

$$\ln (F_1/f_1) = [p - 0.4\kappa'(l/d)]/\kappa'(1 + 0.1 \operatorname{ctg}\alpha). \quad (4)$$

where l_1 is the height of the die parallel for the i-th element of the surface layer; p and α do not have subscripts since they are identical for all elements.

It follows from (4) that for the same f_1 value, the smaller the l_1, the larger the F_1. This means that more metal is directed to the area where the die parallel is smaller. This is a consequence of the well-known law of least resistance[2]. Equation (4) in this case is thus a quantitative expression of this law. Equation (4) relates local metal strain and the length of the parallel. As a result of age hardening, the more plastic strain a metal undergoes, the higher its hardness. According to reference 5

$$HB=ae^b \quad (5)$$

where HB is Brinnell hardness; e, logarithmic strain; a, b, constants whose values are given in reference 4 for different metals.

Substituting equation (4) into (5) we derive the following for logarithmic strain

$$HB_i = a\left[\frac{p - 0.4\kappa' \frac{l_i}{d}}{\kappa'(1 + 0.1 \operatorname{ctg}\alpha)}\right]^b \quad (6)$$

Let us introduce coordinate x along the boundary of the product section. Then a formula for the distribution of metal hardness over the surface of a blank can be derived from (6):

$$HB(x) = a\left[\frac{p - 0.4\kappa' \frac{l(x)}{d}}{\kappa'(1 + 0.1 \operatorname{ctg}\alpha)}\right]^b \quad (7)$$

Substituting (2) into (7), we obtain

$$HB(x) = a\left(\ln \frac{F}{f} + \frac{0.4}{1 + 0.1 \operatorname{ctg}\alpha} \frac{l - l(x)}{d}\right)^b, \quad (8)$$

where l is the average height of the parallel.

It follows from (8) that the height of the parallel has the following distribution for a certain distribution of hardness HB(x) over the surface of

an item:

$$l - l(x) = d\left[\left(\frac{HB(x)}{a}\right)^{1/b} - \ln\frac{F}{f}\right]\frac{1 + 0.1\,\mathrm{ctg}\,\alpha}{0.4}. \quad (9)$$

According to (5), the average value for hardness across the section equals

$HB_{av} = a(\ln F/f)^b$.

Hence we have

$$\ln F/f = (HB_{av}/a)^{1/b} \quad (10)$$

Substituting this equation into formula (9), we obtain

$$l(x) = l - d\left[\left(\frac{HB(x)}{a}\right)^{1/b} - \left(\frac{HB_{cp}}{a}\right)^{1/b}\right]\frac{1 + 0.1\,\mathrm{ctg}\,\alpha}{0.4}. \quad (11)$$

Let us consider the special case of hydraulic extrusion of a square with side 2c. Let us assume that hardness in the item's section increases monotonically from the middle of the side of the square to its apex. Consequently, the maximum height of the parallel should correspond to the middle of the side of the square. Let us label the maximum height of the parallel l_{max} and minimum hardness HB_{min}. Then from equation (1) we have

$$l = l_{max} + d\{[HB_{min}/a]^{1/b} - [HB_{av}/a]^{1/b}\}[(1 + 0.1\ \mathrm{ctg}\alpha)/0.4]. \quad (12)$$

$$l(x) - l_{max} = d\{[HB_{min}/a]^{1/b} - [HB(x)/a]^{1/b}\}[(1 + 0.1\ \mathrm{ctg}\alpha)/0.4]. \quad (13)$$

We obtain the necessary distribution of parallel height[1] by facing the die at its finishing section with a special electrode tool.

To show how the special electrode tool is produced in practice, let us consider the following geometric structure. A cone with angle α at the apex and a surface of rotation coaxial to it given by the formula $Z=\Phi(r)$ are intersected by a plane parallel to the axis. Let us determine distance h between the lines of intersection. Obviously,

$$h(x) = Z_0 + r(x)/\mathrm{tg}\ \alpha - \Phi(r(x)), \quad (14)$$

where r(x) is the square root of (x^2+c^2).

At x = 0 and r = c, distance h becomes maximum

$$h_{max} = Z_0 + c/\mathrm{tg}\alpha - \Phi(r(x)) + \Phi(c). \quad (16)$$

Line 1 in fig. 3 [not reproduced] where the entry cone intersects the plane parallel to the axis models the boundary of the shaping portion of the die.

Line 2 where the surface of rotation intersects the plane models the lower boundary of the parallel. Comparing (13) and (16) we obtain an equation for the surface of rotation that ensures the required distribution of parallel

height:

$$\Phi(r) = \frac{r-c}{\operatorname{tg}\alpha} - d\left[\left(\frac{HB_{min}}{a}\right)^{1/b} - \left(\frac{HB\left(\sqrt{r^2-c^2}\right)}{a}\right)^{1/b}\right]\frac{1+0.1\operatorname{ctg}\alpha}{0.4} \qquad (17)$$

Since $\Phi(c)$ has no effect on the shape of the surface of rotation, $\Phi(c)=0$.

The preliminary die and electrode tool are produced in the following manner.

The die was made by the familiar technology for hydraulic extrusion of a 6 x 6 mm square. The profile was shaped at the exit end of the die on a model 4B723M electroerosion machine by an electrode tool with an equidistant of the size along the contour undersized by 0.1 mm from the size of the finished product. The resulting profile of the die hole along the faces was also undersized 0.04c. Then the electrode tool was set on to a lathe and its entry end faced with a boring tool following the proposed surface shape.

The cutter was sharpened with an optical grinder following a 1:50 scale blueprint pattern of the proposed surface shape. The facing of the end of the electrode tool ended when the cutter touched the edge of the square, i.e. when a circumference with radius r was inscribed into the square.

Figure 3 shows the surface formed by the rotation of the line of the cutting edge of the cutter around axis OZ. This surface of rotation is similar to the sharpened surface of the cutter. When the surface of rotation intersects the plane (face) of the electrode tool, line 1 is formed on the surface of the face of the electrode tool with which the finishing die is faced.

To face profiles, oscillating attachment 4B2723M-116-00 is secured to a 4B723M machine and the electrode tool is fastened to it. After the electrode tool is advanced relative to the profile, which was pre-shaped on the die, the head is assigned a plane parallel movement with an eccentricity of 0.5 mm and simultaneous axial feed. Facing begins when projections 2 on the electrode tool touch the recesses in the die. During this axial feed and plane parallel movement by the electrode tool, only line 1 participates in facing.

Facing ends when apex d of the electrode tool coincides with point d on the die. After profile facing, the entry and finishing portions of the die are brought to the size of the part profile, and the cleanness of the generatrices of the contour of the profile of the finishing portion of the die was raised from class 5 to class 10.

Here is an example of the hydraulic extrusion of a blank into a die made with profiled end facing:

Material - steel 4Kh13; a = 380; b = 0.1; 2c = 6 mm; cross section area of the blank and product - 63 and 36 mm^2; d = 6.8 mm (diameter of the equal-area circle); $\alpha = 20°$ (half angle of die entry).

The necessary minimum hardness of the item after hydraulic extrusion HB_{min} is 340 (specified by the design engineer). Let it be necessary to obtain the following hardness distribution over the sides of the square, i.e.

$HB(x) = 340 + x\,(370-340)/3 = 340 + 10\,x.$

Substituting this equation into (17) we have

$$\Phi(r) = \frac{r-3}{\operatorname{tg} 20^\circ} - 6{,}8\left[\left(\frac{340}{380}\right)^{\frac{1}{0{,}1}} - \left(\frac{340 + 10\sqrt{r^2-9}}{380}\right)^{\frac{1}{0{,}1}} \times \right.$$

$$\left. \times \frac{1 + 0{,}1 \operatorname{ctg} 20^\circ}{0{,}4} \right] + \Phi(r) = (r-3)\,2{,}75 -$$

$$- 21{,}6\left[0{,}329 - \left(\frac{340 + 10\sqrt{r^2-9}}{380}\right)^{10}\right].$$

where r = 3.0, 3.2, 3.4, 4.6, 4.0, 4.2, and 4.24; $\Phi(r)=0$; 3.2, 5.2, 8.9, 10.7, 12.5 and 12.3.

In a die manufactured in this way, pressure was reduced 39 percent, and metal filling along the ribs of the die improved. Hardness on the ribs increased from 320 to 370 HB.

Thus, due to the special ratio of the lengths of the generatrices along the edges and faces, the friction between the blank and the generatrix of the profile was decreased, hardness on the edges of the product was increased, and the quality of the hydraulically extruded items was improved.

References

1. USSR Author's Certificate 1389989, Class B 21 C 25/02. Die for Extruding Shaped Blanks and the Method for Manufacturing It.

2. S. I. Gubkin, "Plasticheskaya deformatsiya metallov" [Plastic Strain of Metals], vol. 3. Moscow, State Publishing House for Ferrous and Nonferrous Metallurgy, 1961, 306 pp.

3. Khill, R., "Matematicheskaya teoriya plastichnosti" [Mathematical Theory of Ductility]. Moscow, State Publishing House for Theoretical Technical Literature, 1956, 407 pp.

4. I. Ya. Tarnovskiy, "Formoizmeneniye pri plasticheskoy obrabotke metallov" [Shape Change During Plastic Processing of Metals]. Moscow, State Publishing House for Ferrous and Nonferrous Metallurgy, 1954, 534 pp.

5. V. A. Krokha, "Krivyye uprochneniya pri kholodnoy deformatsii" [Hardening Curves for Cold Strain]. Moscow, Mashinostroyeniye, 1968, 157 pp.

UDC 621.96.002

Producing Flanged Holes in Sheet Articles

907D0076C Moscow KUZNECHNO-SHTAMPOVOCHNOYE PROIZVODSTVO in Russian No 11, Nov 89 pp 28-29

[Article by A. I. Krater: "Producing Flanged Openings in Sheet Articles"]

[Text] Automotive and agricultural machine building is one of the basic consumers of sheet metal. One way to join sheets is to use flanged holes with and without threading.

A nut-welding method is used to obtain an effective screwing length in a threaded joint. In the other cases, an inseparable joint between parts is made by welding or riveting.

The following processes are used to produce flanged holes:

- flanging small holes with a punch with a sharpened or spherical end;

- flanging medium holes with a stepped punch whose diameter continuously increases in diameter. The first step creates a flange of a specific size , and the next steps gradually increase the height of the flange and make it precise;

- flanging materials to 2 mm thick with simultaneous hole punching or without it;

- flanging holes by puncturing with a nail-shaped punch or joining metal 0.5-0.8 mm thick by riveting.

All flanging methods have in common the fact that precise, high-quality flanged holes are produced without gaps along their edge on the side opposite the direction of the puncture hold so that the burred edge of the hole is less elongated than the rounded edge. This creates major difficulties in producing flanged holes in large parts, and it is almost impossible to make them in small ones that have a closed contour (pipe, rectangular profile, etc.)

A new hole flanging method has been developed[1-3] to produce the precise, high-quality holes with flanging in sheet products and products with a closed contour that are difficult or impossible to produce by existing flanging methods. It involves using the heat of friction that develops when the tool

comes into contact with the piece. In addition to its usual forward movement, the punch also rotates on an axis. The punch's working member is tapered, and the preliminary hole in the piece has the minimum diameter. When it comes into contact with the rotating tool, the piece heats to the specified temperature because of friction, and force P applied to the punch displaces it so that a flange of height (3-4)h forms when the tool advances. It takes 4-5 sec to produce a flanged hole, and the heating zone is local. There is almost no change in the structure of the parts. The punch undergoes special heat treatment to increase durability. Experiments were performed on specimens 0.5-2 mm thick made of different metals in which high-quality flanged holes could not be produced by traditional methods. The research produced equations relating the number of punch rotations to the material thickness, the punch's angle of conicity, the diameter of the specified hole, the coefficients of thermal conductivity, and the heating temperature of the material.

In the proposed flanging process thickness h is much smaller than any sheet dimension. The rotating tool is moved into piece P until it stops, which does not cause ductile flexure. When the tool turns, the sheet material heats at the point where they touch because of friction. This temperature can be set equal to or less than that required for hot die forging.

This heat is used to heat the parts of the die and the piece that are touching. The heat used to heat the rest can be ignored. Zone A, adjacent to the contact surface, is considered the zone of action of a concentrated source. The heat released can be considered heat released by a concentrated source of constant power[4,5] expressed by the equation

$$N=(\lambda/h)F(T_1-T_2) \quad (1)$$

where F is area; h, wall thickness; λ/h, wall thermal conductivity; T_1-T_2, the difference in the temperatures of the top and bottom surfaces of the piece, deg[2,4].

The adequate mechanical power of the concentrated source of the rotating tool[6] is determined from the physical expression of the power of mechanical rotating systems

$$N=P\cdot\cos\alpha\cdot\pi\cdot D\cdot n\cdot\mu, \quad (2)$$

where α is the tool's conicity angle, deg; n, the number of tool rotations, rpm; μ, friction coefficient; D, tool diameter, m; P - force kN[7].

After solving (1) and (2) together and making the necessary mathematical transformations, we derived an equation for determining the number of rotations n of the rotating tool needed to carry out the process

$$n=1.74\lambda\cdot D(T_1-T_2)/P\cdot h\cdot\cos\alpha\cdot\mu \quad (3)$$

The practical application of the process is rather extensive. Depending on the shape of the tool, high-quality holes with flanges can be made in almost any sheet parts, including those with closed contour (pipes, profiles). All these holes after flanging in the form of threading can be used in

disconnecting threaded joints, since the flange surface and the effective screwing length satisfy appropriate requirements.

The process is recommended for metals from 0.3-5 to 2 mm thick, which are widely used in machine building.

References

1. Author's Certificate 637178 Class B21D19/00, Method of Flanging.

2. Author's Certificate 592530 Class B23D51/02, Tool for Making Holes in Plate Parts.

3. Author's Certificate 536339 Class F16B25/00, Self-Shaping and Self-Locking Screw.

4. I. I. Rykalin, "Teplovyye osnovy svarki" [Thermal Basis of Welding]. Moscow, USSR Academy of Sciences, 1947, 185 pp.

5. M. A. Mikheyev, I. M. Mikheyeva, "Osnovy teploperedachi" [Fundamentals of Heat Transfer]. Moscow, Gosenergoizdat, 1860, 206 pp.

6. Tables of Physical Values. Moscow: Fizmatgiz, 1963, 518 pp.

7. S. P. Timoshenko, S. Voynovskiy-Kriger, "Plastiny i obolochki" [Plates and Shells]. Moscow: Fizmatgiz, 1963, 635 pp.

COPYRIGHT: Izdatelstvo, "Kuznechno-shtampovochnoye proizvodstvo"

UDC 621.983.073.001.8

Manufacturing Blanking Dies With Laser Technology, Programmable Control

907D0076D Moscow KUZNECHNO-SHTAMPOVOCHNOYE PROIZVODSTVO in Russian No 11, Nov 89 p 34

[Article by V. L. Akimov, L. V. Vinogradov, S. G. Gornyy, V. A. Lopata: "Manufacturing Blanking Dies with Laser Technology and Numerical Control"]

[Text] A new process for manufacturing shaping the plates of dies and punches of press tooks with complicated shapes and blanking gauges for elastic media has been developed. Cutting edges are contoured using a laser unit which automatically moves the piece and a focused beam relative to one another along a path assigned by the numerical control system.

The blank is a sheet of tool steel or other material subject to finish heat treatment and machining whose thickness ensures the required plate strength and reflects the capabilities of the laser unit. The plates are fixed relative to the die support after laser contouring or before it. In the latter case a more precise product can be obtained. Sheets can be fixed by other methods.

The precision of the resulting tool cutting contour is ±0.01 mm; surface roughness is to Rz=12.5 μ. The process has a capacity of at least 120 pc/hr. It takes no more than 5 min reset the laser unit on a piece of another size.

Capacity increases by a factor of 15 by eliminating fitting and other labor-intensive operations. Tool steel savings are more than 40 percent. New electrophysical hardening methods (laser, plasma, gas detonation, ion implantation, etc,) are used to increase die cutting tool durability. This makes it possible to increase the strength of the die's working several times.

Applications: sheet stamping and the automotive, instrument building, aviation, electrical engineering, electronics, and other branches of industry.

COPYRIGHT: Izdatelstvo, "Kuznechno-shtampovochnoye proizvodstvo"

UDC 621.983.001.8

Press Tool for Punching Holes, Flanging

907D0076E Moscow KUZNECHNO-SHTAMPOVOCHNOYE PROIZVODSTVO in Russian No 11, Nov 89 pp 34-35

[Article by V. A. Romanenko, N. K. Ivanov: "Press Tool for Punching Holes and Flanging"]

[Text] To produce a high-quality flanged hole, one must first cut off excess material and then make the flange. Flanging without punching a hole is possible with small (to 4-5 mm) diameters when the rough edges from the so-called piercing die are on the inner surfaces of the item.

The enterprise designed and produced a press tool[1] for one part. Although the diameter of the flanged hole is 80 mm, there is no blanking die, but the flanged edge has a smooth cut. The figure [not reproduced] shows a general view of the press tool (a) and an axonometric view of a fragment of the punch (b). A spring-loaded puller 2 is fastened to the top plate. Inside it is punch 3. Punch 3 has a flanged step 5, and below its cutting step 6 with interior tapered space 7, framed on its perimeter by cutting teeth 8 with apices 9.

The press tool works as follows: The blank is set onto die 1 (in this case the coordinates determine the elements previously stamped on the die). As the punch descends, the first elements touched are the planes of apex 9 of teeth 8. Holes are punched into the material. Then the waste is cut from the edges of the teeth. Since cutting force includes a vertical and a horizontal constituent and the side to be trimmed is a round-section cantilevered beam with very small overhang, the seemingly inevitable bending does not take place with this arrangement. After cutting, the next step is flanging on the die as the punch descends. The waste is strained and bent along the perimeter. Bends reproduce the alternation of the teeth. The number of punch teeth should be minimum. There were two for a flanging diameter of 18 mm. In this case, because of requirements to reduce the horizontal constituent of cutting force, i.e. to prevent bending during cutting, which degrades cut quality, there were six teeth. Theoretically, there can be two teeth with a large diameter, but then the length of the punch and the press stroke increase since angle α should be no more than 90°. The angle of the interior cone is 60°, the angle of tooth sharpening is 90°. The reduction in tooth sharpening angle improved cut quality, but reduces the strength and wear resistance of the tooth. The press tool's design does not change the rules for calculating the

limit height of the flange[2]. The thickness of the steel sheet that can be processed on this press tool is 0.8 mm.

The press tool can be used on any scale of production. A hole 80 mm in diameter was flanged to install an instrument on a face panel, the blank for which is usually cut on shears, and all holes are punched on a coordinate turret press. The press tool can be installed on such a press. If press tools with fast-change parts are used, one die and one punch can be produced instead of two interchangeable dies and two interchangeable punches, although they will be more complicated. The press tool's design makes it possible to increase labor productivity and eliminate production of the second press tool. The hole does not have to be round.

References

1. USSR Author's Certificate 1328033, class B21D. Press Tool for Notching and Flanging.

2. V. P. Romanovskiy, "Spravochnik po kholodnoy shtampovke" [Handbook on Cold Stamping]. Leningrad: Mashinostroyeniye, 1979.

COPYRIGHT: Izdatelstvo, "Kuznechno-shtampovochnoye proizvodstvo"

UDC 621.979.001.8

Experience Working on Dimensional Presses

907D0076F Moscow KUZNECHNO-SHTAMPOVOCHNOYE PROIZVODSTVO in Russian No 11, Nov 89 pp 35-36

[Article by A. M. Yermolayev, V. V. Nikoforov: "Experience Working on Dimensional Presses"]

[Text] The Minusinsk High-Voltage Vacuum Switch Plant (MZ VV) is successfully operating a material-conserving technology for series production of net-size blanks for parts for vacuum arcing chambers (VAC) such as flanges and vacuum arcing contacts from copper M0b GOST 15741077 and vacuum electric melted copper. The basis for this process is the use of dimensional presses for cubic strain of individual bars or cast blanks of design dimensions to near-net dimensions. These presses were installed on 1,000-kN (model DB2430) and 1600-kN (model DB2432A) hydraulic plastics presses. The previous technology was distinguished by a low material utilization factor due to large margins given the variety of rolled copper goods produced from these grades and to the rather complicated shape of the part. When four kinds of parts were switched to the new technology, rolled copper consumption to produce them dropped 55 percent. In addition to saving raw material, the new process made it possible to lower the labor content of part machining because margins were diminished, individual surfaces of forged pieces did not have to be machined, the grade of rolled copper was standardized, and the structure of the part material was improved, which is critical for vacuum arcing chamber parts. Material savings ranged from 0.14 kg per 0.5-kg part to 2.5 kg per one 2.7-kg part. Labor dropped by 6,000 rated hours, and prime cost decreased more than 100,000 rubles.

The process for manufacturing net-size blanks by straining the initial piece on dimensional presses was recommended to MZ VV by the All-Union Planning and Design Institute for Electrical Production (VPTIElektro, Leningrad). Specialists at the institute's pilot plant produced one 1,000-kN dimensional press and two 1,600-kN dimensional presses for MZ VV and provided technical assistance in introducing the new process. In this work the attempt was made not only to demonstrate the advantages of the new process, but primarily to systematize experience gained during the use of the dimensional stamping (DS) process and identify problems hindering more extensive and more efficient use of this process. Because of the low labor content and prime cost of manufacturing tools, simple adjustment and servicing during operation, high productivity and good part surface quality, the DS technology can be cost-

effective in small series, large series, and mass production.

In the authors' opinion, the following factors are obstructing broader practical use of DS in production:

1. The lack of a uniform procedure which completely reflects the design and manufacturing efficiency of parts produced by DS; of data on the stampability of various materials by DS pressing method which production personnel can use; of techniques for calculating forces and pressing process conditions; of techniques for designing DS tools simple enough for production personnel. Although a rather large amount of work has been published on the capabilities of SF, individual problems have not been dealt with thoroughly enough. At MZ VV, the variety of pieces stamped on dimensional presses can be much larger than that which has been assimilated, but the trial and error method which production engineers use to introduce new parts requires large amounts of time and money and slows the assimilation of DS, especially for parts with rather complicated configuration, where DS produces the maximum effect.

2. The lack of widely disseminated information or data in die forging equipment catalogs on the entire range of dimensional presses which have been developed and field tested and which have proven themselves.

3. At most enterprises, equipment with force only to 1,600 kN (press model PXW-100LA) is produced in series, i.e. for comparatively small parts.

When the DS technology was used at MZ VV the following were identified:

1. The cost-effectiveness of the technology for producing net-size blanks by DS method, which makes necessary a comprehensive study of the capabilities of the DS process and its broader dissemination;

2. The broad technological capabilities of the DS process, the ability to produce non-round, asymmetric, thin-walled parts.

3. The ability and cost-effectiveness of using castings as blanks for DS. For example, MZ VV used blanks cast in a vacuum from copper M06 GOST 15741-77 wastes for one kind of flange with asymmetric axis.

4. DS can be used on DB2330 and DB2432A hydraulic presses for molding plastics, although they are not design for this stringent operating mode. Sometimes they should be updated, and if the DS process becomes sufficiently common, special presses similar to the PXW1-100 should be developed.

5. If an enterprise has traditional cold stamping processes and equipment, DS equipment should be set up in the cold stamping shop, and the cold stamping processes should be designed in combination with the DS process. Figure 3 [not reproduced] shows a one-piece cold-stamped part, previously produced by soldering three parts, in whose manufacture both traditional cold stamping and DS processes were used.

6. While DS is being introduced, precision cutting of the initial piece from bar, e.g. in a differential die, should be introduced. This problem has been

solved for blanks from bar 30 mm in diameter, but for larger diameter bars it represents a definite technological complication and requires separate solution.

7. Problems of mechanizing the loading of the initial blank into the press' working zone and removing the stamped part should be solved when DS is being assimilated by using manipulator robots with the appropriate capcity. When specialized equipment is being developed for DS, the manipulator robot, cartridges, and other accessory equipment should be included.

COPYRIGHT: Izdatelstvo, "Kuznechno-shtampovochnoye proizvodstvo"

UDC 621.791.042

Wire for Buildup of Hot-Deformed Tools

907D0076G Moscow KUZNECHNO-SHTAMPOVOCHNOYE PROIZVODSTVO in Russian No 11, Nov 89 pp 36

[Article by A. I. Urshanskiy, V. A. Anikayev, A. D. Kiselev: "Wire for Buildup of Hot-Deformed Tools"]

[Text] Given the wide variety of metallurgical goods produced in automated production facilities, special requirements are imposed on deforming tools. Increasing the durability and improving the production process for forging dies, hot metal cutting blades, and trimming dies is one effective way to improve the technical and economic indicators of production. Buildup is the most widely used of the promising methods for increasing hot-deforming tool durability.

The use of several types of built-up materials is cost effective when deforming and trimming tools are produced in wide varieties.

The use of buildup wire from carbide-martensite class Np-65Kh3V10MFGT and Np-60Kh5V7M4FGT to restore heavily loaded large rolled tools makes it possible to increase their durability by a factor of 1.5-4.8. The use of these materials is beneficial for press tools, but because of the lack of small-diameter wire, only manual arc buildup is possible. The process of building up tools in this group is difficult to automate because of the complexity of the shape of the die impression to be restored. Existing Np-25Kh10G10T and Sv-08Kh20N9G7T do not provide the necessary heat resistance and stable properties in the built-up metal. Therefore they are not widely used to restore hot-deforming tools.

A new buildup material has been developed: a solid-drawn wire in small diameters with reduced carbide-martensite alloying element content, high heat resistance and manufacturing efficiency. The new material has the additional effect of hardening the built-up metal through the introduction of nitrogen and the later effect of highly concentrated energy sources.

Industrial tests demonstrated the high efficiency of the new buildup material. It is being successfully used for mechanized buildup of pressed inserts and GKM dies in CO_2. As a result of replacing buildup wire Np-65Kh3B10MFGT with the new material, the durability of the dies increased by a factor of 1.5, the cracking rate declined significantly, and the amount of break-off dropped, which prevents the forgings from sticking and premature removal of the tool.

The nature of the wear in the working parts of the die impression changes and shifts toward dimensional wear, in contrast to the fatigue cracks which previously predominated. The absence of deep cracks makes it possible to lower the labor content of machining during later restoration. This is important since the number of restorations usually amounts to several dozen. When the dies of horizontal forging machines were restored during mechanized buildup in shielding gases, productivity increased an average of 25 percent. Because of the decrease in the amount of slag inclusions, conditions for electro-erosion of the die impression improved.

Mechanized buildup of stamped tools made of steels 4Kh5MFS and 7Kh3 in CO_2 was tested to evaluate the performance and manufacturing properties of the new material. About 50 sets of stamped inserts and trimming tools were built up. Tests on the tools under production conditions revealed that the durability of the built-up inserts increased by a factor of 1.6-2.5.

As a result of this work, mechanized buildup of hot-deforming dies was introduced. Commercial production of heat-resistant wire in 1.2, 1.6, 2, 3, 4, and 5 mm diameters has been assimilated.

COPYRIGHT: Izdatelstvo, "Kuznechno-shtampovochnoye proizvodstvo"

- END -

END OF FICHE

DATE FILMED

25 May 90